Journal of Electronic Materials (2022) 51:4133–4138
https://doi.org/10.1007/s11664-022-09722-4

TOPICAL COLLECTION: SYNTHESIS AND ADVANCED CHARACTERIZATION OF MAGNETIC OXIDES

XANES Investigations on Electronic Structure and Magnetic Properties of $GaFeO_3$ Nanocrystals

Aditya Sharma[1] · Mayora Varshney[2] · Tanisha Gautam[1] · Anjali Sharma[1] · Ankush Vij[3] · Ram K. Sharma[4] · Byeong-hyeon Lee[5] · Keun Hwa Chae[5] · Sung Ok Won[5]

Received: 21 February 2022 / Accepted: 18 May 2022 / Published online: 4 June 2022

Abstract

Nanocrystals of $GaFeO_3$ were prepared using co-precipitation followed by thermal annealing at 800 °C for 6 h. The lattice parameters and crystallite size were studied using x-ray diffraction (XRD). Transmission electron microscopy (TEM) measurements were performed to study the size and morphology and revealed the formation of 40–70 nm sized nanoparticles. X-ray absorption near-edge structure measurement was performed to probe the valence state of constituent elements in the $GaFeO_3$ nanocrystals. It has been observed that Fe is present in solely the +3 valence state (i.e., Fe^{3+}). The Ga^{3+} ions are found with vivid distribution at tetrahedral and octahedral sites and the occupancy of Ga^{3+} ions is quantitatively evaluated using Ga K-edge XANES spectra. The low-temperature (50 K) M-H loop measurement conveys a ferrimagnetic character of $GaFeO_3$ compound. The paramagnetic behavior is seen at 300 K. The observed magnetic moments per formula unit (~ 1.6 μ_B) are close to the magnetic moment of Fe^{3+} ions with a low spin state (t_{2g}^5). The abundant Ga^{3+} ions at the tetrahedral site, as confirmed by Ga K-edge XANES analysis, lead to weak anisotropy in the compound and favor the regular hysteresis loop rather the pinched-like hysteresis loop at 50 K.

Keywords $GaFeO_3$ · magnetization · XANES · nanoparticles

Introduction

The metal oxides with magnetic functionalities are the class of materials that obey strong correlations among their electronic/atomic/phase structure and magnetic/optical/catalytic properties.[1–5] The $GaFeO_3$ is a proposed candidate and has been investigated for its catalytic, piezoelectric, and magneto-optic properties.[6–8] The orthorhombic structure of $GaFeO_3$ favors eight formula units per unit cell with diverse distribution of Ga^{3+} and Fe^{3+} ions. The half-fraction of Ga^{3+} ions is surrounded by oxygen tetrahedrons and the other half are surrounded by oxygen octahedrons. The Fe^{3+} ions occupy both tetrahedral and octahedral sites. There is only a single tetrahedral site (Fe4t) in $GaFeO_3$. However, the distribution of Fe^{3+} ions at octahedral sites is more complex because there are two distorted octahedral sites (i.e., Fe1d and Fe2d) and one regular octahedral (Fe3r) site.[9,10] If such complications were not enough in the cation's distribution of the $GaFeO_3$ compound, this is made more complex if the Fe^{3+} ions occupy the Ga^{3+} sites. The complexity in the cation distribution is favorable because of the similar ionic

✉ Aditya Sharma
adityaiuac@gmail.com

✉ Sung Ok Won
sowon@kist.re.kr

1 Department of Physics, Manav Rachna University, Faridabad, Haryana 124001, India

2 Department of Applied Physics, School of Vocational and Applied Sciences, Gautam Buddha University, Greater Noida, Uttar Pradesh 201312, India

3 Department of Physics, University of Petroleum and Energy Studies, Dehradun, Uttarakhand 248007, India

4 Centre for Interdisciplinary Research and Innovation, University of Petroleum and Energy Studies, Dehradun 248007, India

5 Advance Analysis Centre, Korea Institute of Science and Technology (KIST), Seoul 02792, South Korea

radii of Fe^{3+} (0.64 Å) and Ga^{3+} (0.62 Å) ions under the octahedral coordination[9,10] and ultimately depend on the synthesis processes of $GaFeO_3$ crystals. Using the first-principles method, theoretical calculations on $GaFeO_3$ with a different spin and structural configuration have conveyed the antiferromagnetic spin ordering in its ground states.[11,12] Similarly, antiferromagnetic spin configuration is also confirmed by the neutron diffraction studies.[13] On the other hand, substitution of Cr^{3+} ions at octahedrally coordinated Ga^{3+} ions has been reported to have ferromagnetic arrangement towards tetrahedrally coordinated Cr^{3+} ions.[14] However, ideally, unequal distribution of Fe spins of nearly equal magnitude on the sublattices, with a magnetic moment of the spin along the *c* axis, favors the ferrimagnetism in $GaFeO_3$ compound.[15] $GaFeO_3$ finds applications in memory devices, magnetic sensors, and phase shifters.[16–18]

Structural and magnetic properties of pure and doped $GaFeO_3$ compounds are broadly studied in the literature. Nevertheless, to correlate its magnetic interactions, the role of cation distribution, deficiency of certain cations or anions, etc. must be carefully investigated using modern and element-specific characterization techniques such as x-ray absorption spectroscopy (XAS). The conventional electronic structure-determining techniques such as x-ray photoemission spectroscopy (XPS) and Auger spectroscopy are mainly surface-probing techniques and provide electronic structure details of the sub-surface regions. On the other hand, XAS can provide electronic structure properties from the surface and interior of the materials. Therefore, XAS can help to correlate the electronic structure and magnetism in the $GaFeO_3$ compound. In this study, we report on the synthesis of $GaFeO_3$ nanocrystals using sonication-assisted hydrothermal synthesis. Crystal structural, morphology, electronic structure, and magnetic properties are investigated and briefly discussed.

Experimental

All the reagents used were of analytical grade without further purification. For the preparation of the $GaFeO_3$ sample, 3 g of $Ga(NO_3)_3{\cdot}xH_2O$ and 3 g $FeCl_3{\cdot}6H_2O$ were dissolved, separately, in 200 ml ethanol under magnetic stirring. Individual solutions were drizzled into another beaker with additional stirring for 30 min. Subsequent sonication was done for 15 min to obtain a homogeneous solution. The pH of this solution was 4.2. To label the pH of the solution (i.e., pH = 7), 10 mol NH_4OH solution was dropwise added under stirring. Finally, the formed dense precipitates were washed with ethanol and water several times and dried overnight at 80 °C. The dried powder was crushed using a mortar and pestle and annealed at 500 °C for 6 h. Then, the powder was further crushed using the mortar and pestle and again annealed at 800 °C for 6 h. The fine powder was collected carefully by grinding with the mortar and pestle for 30 min. The annealing temperature (800 °C) was determined after confirming the poor crystalline nature of the 500 °C annealed sample by performing the x-ray diffraction measurements. Moreover, a similar annealing temperature has been previously used for the synthesis of $GaFeO_3$ and another metal-oxide compound.[19,20] The dc-magnetization measurements were carried out at 50 K and 300 K using a commercial quantum design physical properties measurement system (PPMS). Transmission electron microscopy (TEM) measurements were performed using a Talos-F200X machine which has capabilities for energy dispersive x-ray (EDX) analysis measurements. O K-edge XANES spectra were collected in total electron yield (TEY) mode at the soft x-ray beamline (10D-XAS-KIST) of the Pohang Accelerator Laboratory (PAL), South Korea. The Fe K-edge and Ga K-edge XANES spectra were collected from the 1D XRS KIST-PAL beamline. The procedure of data collection, use of gas mixtures and typical procedures for the background removal and normalization are provided elsewhere.[21] The x-ray diffraction patterns were collected using a Rigaku-Dmax-2500 x-ray diffractometer with a Cu Kα radiation source (λ = 1.5418 Å). The machine was operated at a tube current of 200 mA and voltage of 40 kV.

Results and Discussion

Figure 1 shows the XRD patterns of prepared samples. The lower and upper panels show the XRD patterns of samples annealed at 500 °C and 800 °C, respectively. It is noticeable from Fig. 1 that the sample annealed at 500 °C shows broad features at ~ 35° and 63°. No intense diffraction peak could be observed in this sample indicating an amorphous or poor crystalline nature. Intense diffraction peaks are observed in the sample annealed at 800 °C indicating a polycrystalline

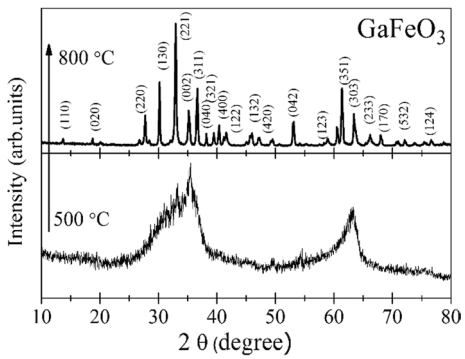

Fig. 1 XRD patterns of $GaFeO_3$. The lower and upper panels show the XRD patterns from 500 °C to 800 °C annealed samples, respectively.

phase formation. All of the diffraction peaks are fairly matched with the previously reported $GaFeO_3$ phase[6,7] and with the standard JCPDF card no. 97-016-7149. Moreover, no diffraction peak was found from the impurity phases of metallic elements (Fe or Ga) or metal oxides (β-Ga_2O_3 or Fe_2O_3). Therefore, the XRD patterns of this study strengthened the formation of a single-phase $GaFeO_3$ compound. The XRD patterns were analyzed with the Powder-X package for evaluating the lattice parameters and full-width at half maxima (FWHM) of the XRD peaks. The XRD patterns have better resembled the experimental XRD patterns when an orthorhombic unit cell (with space group $Pna2_1$) and lattice parameters $a = 8.7413$Å, $b = 9.38955$ Å, and $c = 5.08044$Å and unit cell volume = 416.985 Å^3. The average particle size was evaluated using the Scherrer relation $D = 0.9\lambda/\beta$ Cos θ (λ is the wavelength of the x-rays, D is the crystallite size, β is the FWHM of the diffraction peaks). The estimated size is ~ 50 nm.

Figure 2a shows the TEM images of $GaFeO_3$ annealed at 800 °C. It is seen from the figure that cobbled particles of nearly spherical morphology are present in $GaFeO_3$ annealed at 800 °C. The diffusion of particles is expected under high-temperature annealing which leads to paved particles.[22,23] A few particles are 40 nm in size and others are 70 nm. Figure 2b shows the elemental mapping of the TEM image. There is no populated area of a particular element and thus rules out the formation of metallic clusters of that element. XRD results have also nullified the formation of metallic clusters of constituent elements. Figure 2c shows the EDX profile from the sample. The EDX spectrum provides atomic percentages of individual elements. The Ga, Fe, and O atomic percentages are 19.58, 22.40, and 58.02, respectively. The slightly lower atomic percentage of Ga atoms may arise from the uneven removal of material during the washing/filtering processes. Uneven removal of elements has also been reported for other chemically synthesized oxide systems.[24,25] However, the XRD results showed that the crystal structure and lattice parameters are not much affected by the Ga deficiency. Figure 2d shows the magnified TEM image of the $GaFeO_3$ compound. The lattice of well-defined crystallographic planes is visible and strengthens the high-quality sample preparation under the given synthesis protocols. Figure 2e shows the selected area electron diffraction (SAED) patterns from the sample. It is noticeable that intense patterns of fine dots are visible and indicate the polycrystalline nature of the sample.

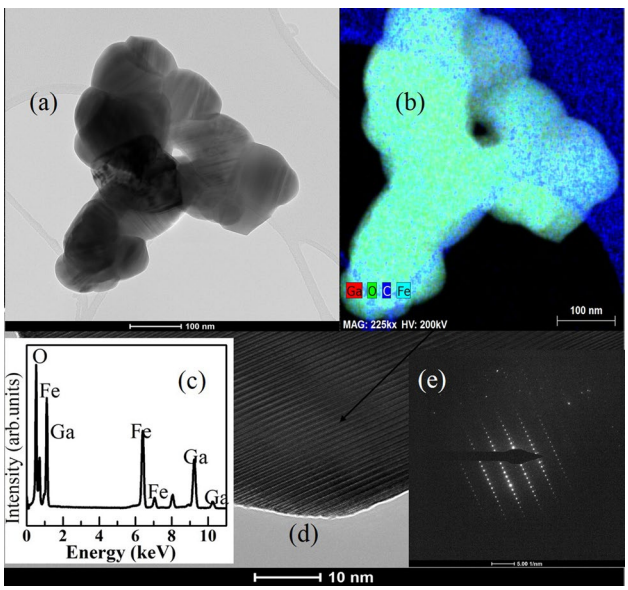

Fig. 2 (a) HR-TEM images of $GaFeO_3$ nanoparticles, (b) elemental mapping profile, (c) EDX spectra, (d) magnified view of $GaFeO_3$ nanoparticles shown in image (a), and (e) SAED patterns of $GaFeO_3$ nanoparticles.

Figure 3 shows the O K-edge XANES of the $GaFeO_3$ compound along with reference β-Ga_2O_3 and Fe_2O_3 compounds. The O K-edge spectrum may be divided into three regions: (i) the pre-edge region ranges from 525 eV to 535 eV, (ii) the white line (main-edge) region ranges from 535 eV to 546 eV and (iii) the post-edge region is from 546 eV and greater. It is noticeable that reference Fe_2O_3 has intense features, especially in the pre-edge region when compared to the reference β-Ga_2O_3 sample. This is because of the basic difference in the electronic configuration of Fe^{3+} ions and Ga^{3+} ions in their respective compounds. In Fe_2O_3, the Fe^{3+} ions obey $3d^5$ electronic configuration and the Ga^{3+} ions possess $3d^{10}$ configuration in β-Ga_2O_3. The pre-edge feature in the Fe_2O_3 sample is due to electronic transitions from O

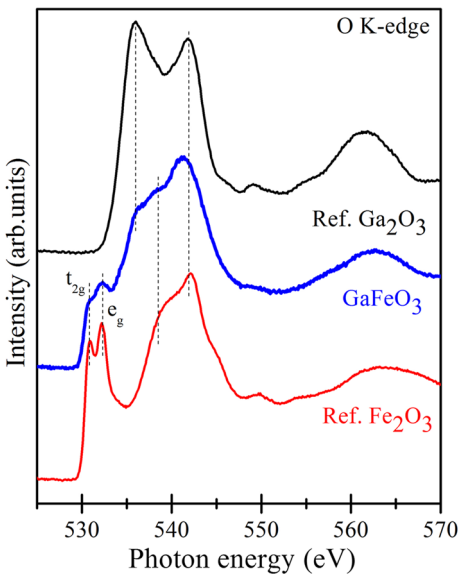

Fig. 3 O K -edge XANES spectra of $GaFeO_3$ nanoparticles along with reference Fe_2O_3 and β-Ga_2O_3.

(1*s*) to the hybridized O (2*p*) and Fe (3*d*) states. The crystal field effects lead to splitting in the pre-edge feature. The first feature (~ 531.0 eV) is called the t_{2g} peak (i.e., group of d_{xy}, d_{xz}, and d_{yz} orbitals) and the second peak (~ 532.0 eV) is due to the e_g feature (i.e., group of d_z^2 and $d_{x^2-y^2}$ orbitals).[26,27] These two features are absent in the O K-edge of the β-Ga_2O_3 sample because there are no significant crystal field effects under the $3d^{10}$ electronic configuration of Ga^{3+} ions. The pre-edge region of the $GaFeO_3$ sample also shows splitting features, namely t_{2g} and e_g. The high intensity of the e_g feature (with a t_{2g}/e_g ratio of 0.95) in the $GaFeO_3$ sample is quite similar to the spectral feature of reference Fe_2O_3 (with a t_{2g}/e_g ratio of 0.94). This indicates that the local environment of Fe^{3+} ions in $GaFeO_3$ is similar to that of Fe_2O_3. The main-edge energy features (between 535 eV and 545 eV, marked by vertical dotted lines) $GaFeO_3$ partly match with the spectral features of Fe_2O_3 and Ga_2O_3 reference samples. This indicates strong hybridization of O 2p and metal (Fe and Ga) 3d orbitals. The other higher energy (545 eV to 570 eV) features correspond to the multiple scattering transitions which may originate from the hybridization of O 2p and metal (n + 1) sp orbitals.

To understand the valence state and hybridization of Fe ions in the $GaFeO_3$ compound, Fe K-edge XANES spectrum is collected and is presented in Fig. 4. For comparison, Fe K-edge spectra are also collected from the Fe foil, FeO, and Fe_2O_3 compounds and are presented in Fig. 4. The Fe K-edge XANES spectrum maps the photo-excited Fe 1s core electrons to the unfilled/partly filled Fe 3*d*/4*p* orbitals.[28,29] A dominating 1*s*→ 4*p* transition, which is electric dipole-allowed, leads to an intense rising-edge feature in the Fe K-edge spectrum.[28,29] The other higher energy spectral features (7150 eV to above) are due to the multiple scattering contribution and originate from Fe 1*s*→ higher *np* states.[28,29] It is noticeable that rising-edge energy position is shifted towards higher energy in the order Fe foil < FeO < Fe_2O_3. This is due to the increase in the oxidation of Fe ions in the reference samples.[28,29] The rising-edge, white line peak and spectral features (up to 7400 eV) of the $GaFeO_3$ sample closely match with the features of Fe_2O_3 samples. This suggests that the oxidation state of Fe ions in $GaFeO_3$ is similar to the Fe ions of the Fe_2O_3 sample (i.e., Fe^{3+} ions). However, the multiple scattering peaks (above 7175 eV) of Fe_2O_3 and $GaFeO_3$ compounds are diverse and indicate the different coordination chemistry of Fe^{3+} ions in these two compounds.

Figure 5a shows the normalized Ga K-edge spectra of β-Ga_2O_3 and $GaFeO_3$ samples. The Ga_2O_3 compound obeys Ga^{3+} ions with diverse distribution at tetrahedral and octahedral sites.[30–33] It is noticeable from Fig. 5a that rising-edge energy position of both compounds mimic each other and strengthen the presence of dominant Ga^{3+} ions in both compounds. The spectral features are diverse in the white-line region (10365 eV to 10375 eV). The white-line region of the β-Ga_2O_3 sample exhibits a flat plateau. On the other hand, the white-line peak exhibits two features at 10368.5 eV and 10372 eV, respectively. The low-energy spectral feature (at 10368.5 eV) is ascribed to tetrahedral coordinated Ga^{3+} ions and the high-energy feature (at 10372 eV) is due to the octahedrally coordinated Ga^{3+} ions.[30,31] β-Ga_2O_3 exhibits equal distribution of Ga^{3+} ions at tetrahedral and octahedral

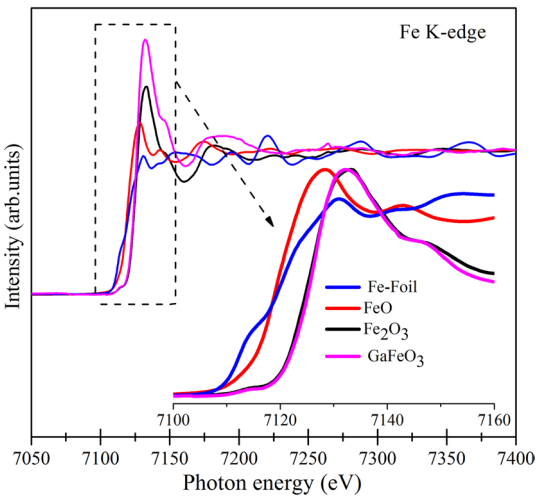

Fig. 4 Fe K-edge XANES spectra of $GaFeO_3$ nanoparticles along with reference Fe foil, FeO and Fe_2O_3.

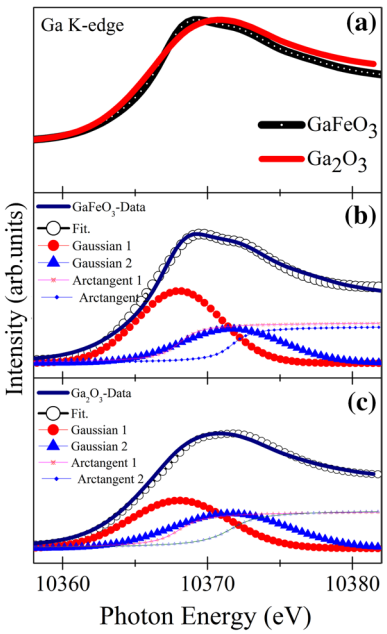

Fig. 5 (a) Ga K -edge XANES spectra of $GaFeO_3$ nanoparticles and β-Ga_2O_3. (b) and (c) show the fitting of Ga K-edge white line peak for determining the quantitative occupancy of Ga^{3+} ions at tetrahedral and octahedral sites.

positions, and other phases of gallium oxide have exhibited clear distribution of Ga^{3+} ions at tetrahedral and octahedral sites.[30,31] In the present case, for the $GaFeO_3$ sample, we have estimated the quantitative distribution of Ga^{3+} ions at tetrahedral and octahedral sites using the standard procedure adopted in previous reports[30,31] which are presented in Fig. 5b. Briefly, to evaluate the fraction of tetrahedral occupancy Ga(t)% and a fraction of octahedral occupancy Ga(o)%, we have applied the area ratios in the following manner:

$$\mathrm{Ga}(t)\% = \frac{\text{Area of Gaussian 1}}{(\text{Area of Gaussian 1} + \text{Area of Gaussian 2})} \times 100$$

$$\mathrm{Ga}(o)\% = \frac{\text{Area of Gaussian 2}}{(\text{Area of Gaussian 1} + \text{Area of Gaussian 2})} \times 100$$

The estimated Ga(t)% and Ga(o)% are 58.12 and 41.88, respectively. It is clear that the tetrahedral sites are more favorable for Ga^{3+} ions in $GaFeO_3$ compound. Similarly, from Fig. 5c, the Ga(t)% and Ga(o)% for the reference β-Ga_2O_3 are estimated as 52.1 and 47.9, respectively, which is close to the previous reports.[30–32]

To understand the magnetic properties of the $GaFeO_3$ compound, low-temperature (50 K) and room-temperature (300 K) magnetic field versus magnetization (M-H) measurements are performed and are presented in Fig. 6. It is noticeable that the low-temperature (50 K) M-H loop has a ferrimagnetic character which is analogous to the previous reports.[14,15] It is observed from Fig. 6a that the magnetization increases rapidly in the low-field regime (0–0.8 T) and reaches ~ 36 emu/g. The magnetization increases slowly in the applied-field regime of 1 T to 3 T and nearly saturates to ~ 50 emu/g when the maximum applied field is 5 T. In most of the previous reports, the M-H data of $GaFeO_3$ samples have shown a pinched-like hysteresis loop.[11,34] These pinched-like loops with different coercivities were explained in terms of two additive loops of two-phase systems. The three cations at octahedral sites (i.e., two Fe^{3+} ions and one Ga^{3+} ion) have strong anisotropy, whereas the tetrahedrally coordinated Ga^{3+} ions obey weak anisotropy. Hence, these sets of octahedrally and tetrahedrally coordinated ions act as hard and soft magnetic phases, respectively. Moreover, it was also anticipated that the magnetic properties are adjusted by the site disorder of cations which are indeed subjected to the applied synthesis protocols.[11] In the present case, the Ga K-edge XANES spectra revealed higher occupancy at tetrahedral sites of Ga^{3+} ions and suggest weak anisotropy in the compound. The higher occupancy at tetrahedral sites is possible if we anticipate that a few Ga^{3+} ions, which could be present at the octahedral site, are removed during the synthesis process and evidenced by the EDX study (as the low stoichiometry of Ga; see Fig. 2c). The calculated the magnetic moment per formula unit of $GaFeO_3$ and is ~ 1.6 μ_B. As stated above, the Ga^{3+} ions do not contribute to the net magnetization of the $GaFeO_3$ compound because unpaired electrons are unavailable under the $3d^{10}$ electronic configuration of Ga^{3+} ions. Therefore, the Fe^{3+} ions are anticipated as a source of magnetization in $GaFeO_3$. It is also known that the Fe^{3+} ($3d^5$) ions possess a magnetic moment of ~ 5.91 μ_B for a high spin state (t_{2g}^3, e_g^2). The calculated magnetic moment per formula unit of the $GaFeO_3$ compound is ~ 1.6 μ_B, which is far below the spin-only moments of Fe^{3+} ions under the high-spin configuration. However, the calculated magnetic moment of $GaFeO_3$ (~ 1.6 μ_B) is comparable to the magnetic moments of Fe^{3+} ions under the low spin state (t_{2g}^5, 1.73 μ_B) and suggests the presence of low spin state Fe^{3+} ions in the $GaFeO_3$ compound prepared under the given protocols. It is also noticeable from Fig. 6a that the coercivity of $GaFeO_3$ (at 50 K) is 0.44 T which is also comparable to the previously reported values.[11,34] Figure 6b shows the room temperature MH loop of $GaFeO_3$ compound. It is noticeable from Fig. 6b that the magnetization completely disappeared, and a typical paramagnetic ordering is observed. It is known that the transition temperature of $GaFeO_3$ is ~ 220 K; therefore, at room temperature, the compound exhibits paramagnetic properties.[11,34] Overall, at 50 K, the observed high saturation magnetization and coercive field confirm the robust ferrimagnetic nature of the $GaFeO_3$ compound and may be useful for designing spintronic devices to switch the magnetic ordering with a small external magnetic field. Hence, it can be concluded that the $GaFeO_3$ compound

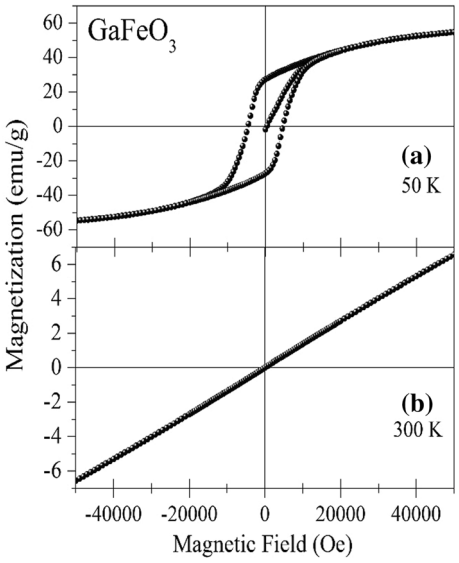

Fig. 6 Magnetic field versus magnetization data of $GaFeO_3$ nanoparticles measured at (a) 50 K and (b) 300 K.

exhibits ferrimagnetic behavior below room temperature, where the abundant Ga^{3+} ions at the tetrahedral site lead to weak anisotropy in the compound and favor the regular hysteresis loop rather the pinched-like hysteresis loop reported in previous studies.[11,34]

Conclusions

Single-phase $GaFeO_3$ nanocrystals are prepared using co-precipitation and subsequent annealing. HR-TEM images with SAED patterns depict the formation of 40–70-nm-sized particles with high crystallinity. XANES spectra at Fe K-edge and Ga K-edge confirm the Fe^{3+} ions and Ga^{3+} ions in the $GaFeO_3$ compound. Quantitative analysis of Ga K-edge XANES confirms the higher percentage of Ga^{3+} ions at tetrahedral sites. $GaFeO_3$ nanoparticles possess a magnetic moment of ~ 1.6 μ_B per formula unit and coercivity of 0.44 T at 50 K. Higher concentration of Ga^{3+} ions at the tetrahedral site leads to weak anisotropy in $GaFeO_3$ nanoparticles and favors the regular hysteresis loop. The ferrimagnetic properties vanish at room temperature because of its natural transition temperature at 220 K.

Acknowledgment Dr. Aditya Sharma is thankful to the Honorable Vice-Chancellor and Dean(s) of the Manav Rachna, University, Faridabad, for constant support and encouragement.

Conflict of interest The authors declare that they have no conflict of interest.

References

1. X. He, X. Song, W. Qiao, Z. Li, X. Zhang, S. Yan, W. Zhong, and Y. Du, *J. Phys. Chem. C* 119, 9550 (2015).
2. A. Sharma, M. Varshney, J. Park, T.K. Ha, K.H. Chae, and H.J. Shin, *RSC Adv.* 5, 21762 (2015).
3. H. van Gog, W.F. Li, C. Fang, R.S. Koster, M. Dijkstra, and M. van Huis, *NPJ 2D Mat. Appl.* 3, 18 (2019).
4. M.S. Chavali, and M.P. Nikolova, *SN Appl. Sci.* 1, 607 (2019).
5. Y. Zhu, X. Zhang, K. Koh, L. Kovarik, J.L. Fulton, K.M. Rosso, and O.Y. Gutiérrez, *Nat. Commun.* 11, 3269 (2020).
6. V.S. Kujur, and S. Singh, *J. Mater. Sci: Mater. Electron.* 31, 17633 (2020).
7. A.M. Kalashnikova, R.V. Pisarev, L.N. Bezmaternykh, V.L. Temerov, A. Kirilyuk, and Th. Rasing, *Jetp Lett.* 81, 452 (2005).
8. S.C. Abrahams, J.M. Reddy, and J.L. Bernstein, *J. Chem. Phys.* 42, 3957 (1965).
9. T. Arima, D. Higashiyama, Y. Kaneko, J.P. He, T. Goto, S. Miyasaka, T. Kimura, K. Oikawa, T. Kamiyama, R. Kumai, and Y. Tokura, *Phys. Rev. B* 70, 064426 (2004).
10. M.J. Han, T. Ozaki, and J. Yu, *Phys. Rev. B* 75, 060404(R) (2007).
11. S.G. Bahoosh, and J.M. Wesselinowa, *J. Appl. Phys.* 113, 063905 (2013).
12. J. Atanelov, and P. Mohn, *Phys. Rev. B.* 92, 104408 (2015).
13. S. Basu, R. Singh, A. Das, T. Roy, A. Chakrabarti, A.K. Nigam, S.N. Jha, and D. Bhattacharyya, *J. Phys. Chem. C* 119, 2029 (2015).
14. T. Katayama, S. Yasui, T. Osakabe, Y. Hamasaki, and M. Itoh, *Chem. Mater.* 30, 1436 (2018).
15. H. Niu, M.J. Pitcher, A.J. Corkett, S. Ling, P. Mandal, M. Zanella, K. Dawson, P. Stamenov, D. Batuk, A.M. Abakumov, C.L. Bull, R.I. Smith, C.A. Murray, S.J. Day, B. Slater, F. Cora, J.B. Claridge, and M.J. Rosseinsky, *J. Am. Chem. Soc.* 139, 1520 (2017).
16. J. Zhai, N. Cai, Z. Shi, Y. Lin, and C.W. Nan, *J. Phys. D Appl. Phys.* 37, 823 (2004).
17. C.W. Nan, N. Cai, L. Liu, J. Zhai, Y. Ye, and Y. Lin, *J. Appl. Phys.* 94, 5930 (2003).
18. K. Zhao, K. Chen, Y.R. Dai, J.G. Wan, and J.S. Zhu, *Appl. Phys. Lett.* 87, 1629011 (2005).
19. A. Sharma, S. Kumar, R. Kumar, M. Varshney, and K.D. Verma, *Opto. Electr. Adv. Mater. Rap. Commun.* 3, 1285 (2009).
20. K. Recko, U. Wykowsk, W. Olszewski, G. Andre, J.J. Milczarek, D. Satula, M. Biernacka, B. Kalska-szostko, J. Waliszewski, and K. Szymanski, *Opto. Electr. Adv. Mater.* 17, 1173 (2015).
21. A. Sharma, J.P. Singh, S.O. Won, K.H. Chae, S.K. Sharma, and S. Kumar, *Handbook of Materials Characterization* (New York: Springer, 2018), p. 497.
22. A. Sharma, M. Varshney, K.H. Chae, and S.O. Won, *RSC Adv.* 8, 26423 (2018).
23. M. Varshney, A. Sharmaa, K.H. Chae, S. Kumar, and S.O. Won, *J. Phys. Chem. Sol.* 119, 242 (2018).
24. G. Ye, G. Oprea, and T. Tom, *J. Am. Ceram. Soc.* 88, 3241 (2005).
25. V.K. Singh, and R.K. Sinha, *Mater. Lett.* 31, 281 (1997).
26. J.G. Chen, *Surf. Sci. Rep.* 30, 1 (1997).
27. A. Sharma, M. Varshney, H.J. Shin, Y.J. Park, M.G. Kim, T.K. Ha, K.H. Chae, and S. Gautam, *Phys. Chem. Chem. Phys.* 16, 19909 (2014).
28. J.P. Singh, B. Kaur, A. Sharma, S.H. Kim, S. Gautam, R.C. Srivastava, N. Goyal, W.C. Lim, H.J. Lin, J.M. Chen, K. Asokan, D. Kanjilal, S.O. Won, I.J. Lee, and K.H. Chae, *Phys. Chem. Chem. Phys.* 20, 12084 (2018).
29. A. Sharma, M. Varshney, Y. Kumar, B.H. Lee, S.O. Won, K.H. Chae, A. Vij, R.K. Sharma, and H.J. Shin, *J. Phys. Chem. Sol.* 161, 110476 (2022).
30. K. Nishi, K.I. Shimizu, M. Tanamatsu, H. Yoshida, A. Satsuma, T. Tanaka, S. Yoshida, and T. Hattori, *J. Phys. Chem. B* 102, 10190 (1998).
31. K.I. Shimizu, M. Tanamatsu, K. Nishi, H. Yoshida, A. Satsuma, T. Tanaka, S. Yoshida, and T. Hattori, *J. Phys. Chem. B* 103, 1542 (1999).
32. A. Sharma, M. Varshney, H.J. Shin, K.H. Chae, and S.O. Won, *RSC Adv.* 7, 52543 (2017).
33. A. Sharma, M. Varshney, H. Saraswat, S. Chaudhary, J. Parkash, H.J. Shin, K.H. Chae, and S.O. Won, *Int. Nano Lett.* 10, 71 (2020).
34. T.C. Han, T.Y. Chen, and Y.C. Lee, *Appl. Phys. Lett.* 103, 232405 (2013).